Optimization of an urban monitoring network for emergency response applications: An approach for characterizing the source of hazardous releases

Pierre Ngae, Hamza Kouichi, Pramod Kumar, Amir Ali Feiz, Amer Chpoun

Optimization of an urban monitoring network for emergency response applications: An approach for characterizing the source of hazardous releases

Pierre Ngae | Hamza Kouichi | Pramod Kumar | Amir-Ali Feiz | Amer Chpoun

LMEE, Université d'Evry Val-d'Essonne, Courcouronnes, France

Correspondence
Hamza Kouichi, LMEE, Université d'Evry Val-d'Essonne, 40 Rue du Pelvoux, 91020 Courcouronnes, France.
Email: hamza.kouichi@univ-evry.fr

The aim of this study is to optimize sensor networks for fast deployment in order to reconstruct an unknown source of intentional or accidental release in local urban topography. In such emergency circumstances, only the meteorological conditions are available in real time and the network deployed must be efficient enough regardless of a source's position and intensity. To determine the optimal positions to be instrumented by the sensors, an adequate cost function is defined based on the *renormalization* inversion method. This function, named the *entropic criterion*, quantifies the amount of information contained in a network of the sensors to estimate the intensity and the location of an unknown source. The optimal design is approached as combinatorial optimization (NP-Hard) and a stochastic algorithm (simulated annealing, SA) is employed to solve this problem. The computation is performed by coupling the CFD adjoint fields in an urban environment, the renormalization algorithm and the SA. The optimization is evaluated with 20 trials of the Mock Urban Setting Test (MUST) tracer field experiment for the reconstruction of a continuous point release in an idealized urban geometry using optimal networks of sizes 10 and 13 sensors. The process is achieved successfully and the results showed that the reduction of an original network of 40 sensors to one third (13) and one quarter (10) does not degrade the performance of this network. Also, a comparison of the optimal design efficiency based on *a priori* information and without *a priori* information about the source showed that the present entropic criterion leads to network design and performance that can accurately retrieve an unknown emission source in an urban environment.

KEYWORDS

monitoring network optimization; source term estimation; CFD; renormalized inversion; simulated annealing

1 | INTRODUCTION

Reconstruction of the air contamination origin at local scale is an important operational issue for local authorities, public health professionals, industrial sites, security and defence authorities, etc. In fact, a source (leak, terrorist attack, etc.) identification can provide on-site assistance for managing the emergency, supporting the decisions, neutralize the danger and refurbishment of the installations. As the issue is crucial, estimation of the source parameters (i.e. intensity and position) must be precise. To ensure that, an established monitoring network plan must be optimal and the sensor locations must be well chosen to address the situation.

In the case of an emergency, only meteorological conditions can be known in real time from the available observations or from numerical weather forecasting models; *a priori* information about the pollutant source is generally not available. However, in this study each meteorological situation is assumed as stationary and described by regional wind speed and direction and stability class. Here a great challenge is

to design an optimal sensor network for an unknown source estimation but without any information from the source. This context of emergency responses concerns an optimal strategy for sensor deployment for a specific meteorological condition. An example of networks concerned by this kind of optimization study is the sensor networks carried by mobile systems (e.g. robots or drones) deployed only in emergency situations. In this context, the optimization of the network can be performed:

(a) *In real time* if the area of interest is not complex and the calculation can be conducted quickly in a very short time, using for example, the Gaussian dispersion model and an optimization algorithm (Ma *et al.*, 2013).

(b) *In upstream off-line* if the domain is complex (i.e. contains several obstacles), a computational fluid dynamics (CFD) model can be used to include the effect of the obstacles.

Several studies have been conducted for the optimization of the monitoring networks using optimization algorithms (Ko *et al.*, 1995; Jiang *et al.*, 2007; Abida *et al.*, 2008; Abida and Bocquet, 2009; Saunier *et al.*, 2009; Ma *et al.*, 2013; Efthimiou *et al.*, 2017; Kouichi, 2017). Recently, Ma *et al.* (2013) and Kouichi *et al.* (2018) described the optimization methodologies for designing optimal monitoring networks in homogeneous and urban regions, respectively. In these studies, concentration measurements were utilized in the optimization process to determine the optimal configurations of the networks. However, *a priori* information about the source is generally not available for the deployment of the sensors in an optimal way, since in some scenarios the source information is unknown before an accident happens. Therefore, these methods may have limitations since they depend on both source information and meteorological conditions. Thus, it is essential to develop methodologies for an optimal sensor network using only the available meteorological conditions and which do not require the *a priori* source information.

The optimality criterion can be based on the characteristics of the networks. For examples, Caselton *et al.* (1992), Le and Zidek (1994), and Zidek *et al.* (2000) used information contained in the sensor networks. The optimal design of networks by Nychka and Saltzman (1998), Dhillon and Chakrabarty (2003), Altinel *et al.* (2008), Wu *et al.* (2008), and Mini *et al.* (2011) were based on the spatial distribution of the sensors in the domain. Mason and Bohlin (1995) and Hourdin and Issartel (2000) used the probability of detection to design the monitoring networks. In the present study, the cost function for the optimization of a monitoring network is inspired by the concept of information theory (Shannon and Weaver, 1998) and it is defined from the *renormalization* inversion method (Issartel, 2005). This *entropic criterion* can quantify the amount of information contained in a network and is useful for the source reconstruction. A great advantage of this method for designing the optimal networks is that it is purely based on the meteorological conditions and *a priori* information on the source is not required. The concentration measurements from an optimal network obtained from this methodology are utilized for the reconstruction of an unknown continuous point source in an urban-like environment.

The reconstruction of an unknown release from a finite set of measurements is the topic of great importance for the Source Term Estimation (STE) problem. Rao (2007) and more recently Hutchinson *et al.* (2017) provided a detailed overview of the different methods. These methods can be classified in three major categories: the probabilistic, the deterministic and the hybrid. The probabilistic category treats the source parameters as random variables associated with probability distributions. This includes the Bayes Estimation Theory (Monache *et al.*, 2008; Luhar *et al.*, 2014), Monte Carlo algorithms using Markov chains (MCMC; Keats, 2009; Yee *et al.*, 2014) and various stochastic sampling algorithms (Zhang *et al.*, 2015). Deterministic methods and other data assimilation techniques use cost functions to assess the difference between the observations and the modelled measurements and are based on the iterative processes to minimize this gap (Seibert, 2001; Kaminski and Heimann, 2001; Davoine and Bocquet, 2007; Sharan *et al.*, 2009; Kovalets *et al.*, 2011). In this study, the renormalization inversion technique (Issartel, 2005) is utilized to develop an algorithm for the optimization of sensor networks and also for the source reconstruction process. This inversion method is operational and efficient for the source estimation at local and continental scale and also in different terrain topography (i.e. domains with and without obstacles) (Issartel, 2005; Sharan *et al.*, 2009); Kumar *et al.* 2015b; 2016). Recently, the renormalization technique was coupled with optimization algorithms (simulated annealing and genetic algorithm) for the optimal design of networks and the results were satisfactory (Kouichi *et al.*, 2016; Kouichi, 2017).

The objective of this study is to present a methodology to optimize sensor networks for emergency situations and for mobile network deployment (Lepley and Lloyd, 2010; Lepley *et al.*, 2011) in order to reconstruct an unknown emission source at local scale and in urban environments. The presented methodology does not require any information from the source for the optimization process. The optimization is performed by coupling CFD adjoint fields that evaluate the sensitivity of the sensors in an urban domain, the renormalization algorithm and the SA algorithm. To evaluate this methodology, the data from the Mock Urban Setting Test (MUST) tracer field experiment (Biltoft, 2001; Yee and Biltoft, 2004) is utilized. This dataset represents the results of an experimental campaign using a point release in a urban-like environment in various atmospheric stability conditions.

2 | METHODOLOGY: OPTIMAL DESIGN OF THE SENSOR NETWORK

As the measurements can only be performed at a limited number of locations in space, the optimal design of a sensor network consists in finding the "best" subset of m positions

in the implementation area where p candidate positions are dispersed. Here, the possible numbers of m combinations from a given set of all p positions are C_m^p. It is obvious that if p is large, the problem is NP-Hard (Non-deterministic Polynomial-time hardness) as shown by Ko *et al.* (1995). If a set of the potential positions of sensors is given by $\mathbf{X}^r = (x_i^r, y_i^r)_{i=1,..p}$ at a fixed vertical height above the ground surface in two-dimensional Cartesian coordinates $\mathbf{x} = (x, y)$, a network N can be defined by the set $\mathbf{X} = (x_i, y_i)_{i=1,..m}$ of m positions. The "best" network N^{o} defined by a set $\mathbf{X}^{\mathrm{o}} = (x_i^{\mathrm{o}}, y_i^{\mathrm{o}})_{i=1,..m}$ of m positions among the possible subsets $\mathbf{X}$ is the optimal network. Finding N^{o} is named a *Combinatorial Optimization Problem*. The search for N^{o} was performed by the minimization (or maximization) of a cost function which describes quantitatively the quality of the network.

In a case when the p candidate positions are not predefined, the optimization of sensor networks is part of the "first deployment" problem. This problem is more complex than updating the arrangement of a set of sensors already placed or reducing or increasing the size of an existing network where *a priori* information is available. The first deployment can be solved by two main steps:
(a) Definition of the different studied areas (the danger area where a source can be located, the vulnerable area that needs to be protected against contamination and the instrumented area where the sensors will be implanted), and
(b) Definition of the potential positions for sensor implantation; this step can be solved by assigning a weight of danger to each point in the areas of interest and by using as additional information the sensor detection threshold, the threshold exposure limits (e.g. National Research Council, 2010 on acute exposure guidelines for selected airborne chemicals), and the time limits of exposure.

If *a priori* information of the optimal networks sizes is not available, defining m is also a part of the optimization problem and it can be declared as a variable that changes (increases or decreases) randomly during the optimization process. This increases considerably the search space and the time of optimization. Also this means that the selected optimization algorithm must be independent of the scale of the cost function because the comparison will be for networks of different sizes, thus of different cost scales. This can also increase the complexity of the parametrization of the optimization algorithms. A second methodology consists of performing an initial optimization for the networks of different sizes (as example from 3 to $p/2$) in order to determining the optimal size (Kouichi, 2017).

2.1 | Cost function

In order to obtain the optimal network, an appropriate cost function is required. This cost function is defined according to the objective of the "network design", and it quantifies the quality of a specific network. As in this study the optimization is for the reconstruction of the origin of atmospheric releases without using *a priori* information on the source, the cost function is defined based on the concept of *illumination* introduced by Issartel (2005). This concept was originally proposed to develop a deterministic inversion technique based on the adjoint approach and allows us to evaluate the resolution in a monitored area by quantifying which part of a domain is well, poorly or not at all seen (Issartel, 2005). The retroplumes (i.e. adjoint fields) calculated from the sensors, assign to each point in the monitored area a level of illumination that can be interpreted as the probability of detection. For ordinary adjoint fields, the illumination is excessive close to the sensors and the inversion artifacts (i.e. the artificial information included in the inversion methodology) are corrected by attributing for each point of the domain an optimal weight. This correction is realized by a weight function, $f(\mathbf{x})$, that prevents any overestimation in interpretation of the observations that would lead to the artifacts. The computation of $f(\mathbf{x})$ is based on the adjoint functions, $a_i(\mathbf{x})$ (Pudykiewicz, 1998; Issartel, 2005) which evaluate the sensitivity of the ith receptor in a domain Ω. The adjoint functions (or fields), called retroplumes, are obtained by an atmospheric dispersion model in the backward mode and by considering the detector as a pseudo-point source of unit intensity (Issartel and Baverel, 2003; Hourdin and Talagrand, 2006). For m receptor locations in a domain, $\mathbf{a}(\mathbf{x}) = [a_1(\mathbf{x}), a_2(\mathbf{x}), ..., a_m(\mathbf{x})]^{\mathrm{T}}$. In the renormalization inversion method, the adjoint fields are optimally weighted by introducing a suitable positive weight function $\phi(\mathbf{x})$, which is computed as the converged value of a function $f_k(\mathbf{x})$ using the following iterative algorithm (Issartel, 2005):

$$f_{k+1}(\mathbf{x}) = f_k(\mathbf{x}) \sqrt{\mathbf{a}_{f_k}^{\mathrm{T}}(\mathbf{x}) \mathbf{H}_{f_k}^{-1} \mathbf{a}_{f_k}(\mathbf{x})}, \quad f_0 = 1, \tag{1}$$

where, for an iteration number k, $a_{f_i}(\mathbf{x}) = a_i(\mathbf{x})/f_k(\mathbf{x})$ is the transformed weighted adjoint functions and thus $\mathbf{a}_{fk}(\mathbf{x}) = \mathbf{a}(\mathbf{x})/f_k(\mathbf{x})$. $\mathbf{H}_f$ is the weighted *Gram* matrix defined by:

$$\mathbf{H}_f = \int_\Omega \mathbf{a}_f^{\mathrm{T}}(\mathbf{x}) \mathbf{a}_f(\mathbf{x}) f(\mathbf{x})\, \mathrm{d}\mathbf{x} \tag{2}$$

The visibility function $\phi(\mathbf{x})$ (i.e. converged value of $f(\mathbf{x})$) satisfies the following three conditions (Issartel, 2005):

$$\text{(i)}\ \ \phi(\mathbf{x}) > 0, \ \ \text{(ii)}\ \int_\Omega \phi(\mathbf{x}) \mathrm{d}\mathbf{x} = m, \ \ \text{(iii)}\ \ \mathbf{a}_\phi^{\mathrm{T}}(\mathbf{x}) \mathbf{H}_\phi^{-1} \mathbf{a}_\phi(\mathbf{x}) \equiv 1. \tag{3}$$

The condition (iii) is often named the renormalization condition and presents a stopping criterion of the iterative process.

Issartel (2005) noticed that $\phi(\mathbf{x})$ corresponds to an entropic criterion that quantifies the optimal amount of information contained in a network for the inversion process. Based on the concept of information theory (Shannon and Weaver, 1998) and by interpreting the weighted Gram matrix $\mathbf{H}_\phi$ (Equation 2) as a covariance matrix of the Gaussian distribution for m measurements, Issartel (2005) defined the entropy

S_f associated with an ordinary weight function f as:

$$S_f = \frac{m}{2}\log(2\pi) + \frac{1}{2}\log(\det \mathbf{H}_f). \quad (4)$$

By selecting a unique optimal weight function $\phi(\mathbf{x})$ and in order to not overestimate the observations, this quantity S_f of information added to the inverse process should be minimized. The entropy-based cost function is a characteristic of a given network and evaluates the amount of information contained in the network in order to reconstruct an unknown release in a region. Since m is a constant, the first term in Equation 4 can be neglected and thus the minimum of S_f corresponds to the minimum of $\log(\det \mathbf{H}_f)$. Consequently, the optimal entropic criterion that verifies the optimal weight function $\phi(\mathbf{x})$ (Equation 3) for source reconstruction, can be evaluated as:

$$S_\phi = \frac{1}{2}\log(\det \mathbf{H}_\phi). \quad (5)$$

S_ϕ in Equation 5 is a scalar that depends only on the meteorological conditions and the sensors' sensitivity in the monitored area. Since $\phi(\mathbf{x})$ is unique, the optimal weighted Gram matrix $\mathbf{H}_\phi$ is also unique and described for a given network of the sensors distribution in a domain. As in some emergency situations after an intentional or accidental release, only the meteorological conditions are available (i.e. average wind speed and direction, stability class), the entropic criterion (Equation 5) is selected for designing the optimal monitoring network. This cost function is independent from the concentration measurements and does not require any information on the source. It is clear that if the source to be located in a large domain without *a priori* information about it, the amount of information contained in the monitoring network defined according to a given meteorological situation must be maximized in order to cover a potentially large space. Therefore, the optimal network N^{o} in a search space (I) formed by all the possible combinations C_m^p, is obtained by maximizing S_ϕ (Equation 5) and it verifies:

$$\text{(a)}\ \ S_\phi(N^0) = \max_{N\subset I} S_\phi(N), \qquad \text{(b)}\ \ N^0 = \arg\max_{N\subset I} S_\phi(N). \quad (6)$$

2.2 | Optimization algorithm

Regardless of the optimality criterion, the feasibility of the computations is an important challenge in a network optimization problem. The computation time to find an optimal solution by exhaustive search becomes forbiddingly large when the size of the instances grows (depending on the time for the calculation of the cost function and the number of the possible combinations). To solve such problem, stochastic algorithms are efficient and among them simulated annealing (SA) is recommended in the literature (Jiang *et al.*, 2007; Abida *et al.*, 2008; Abida and Bocquet, 2009; Saunier *et al.*, 2009). This probabilistic algorithm explores stochastically the search space and converges iteratively to the solution (Metropolis *et al.*, 1953). For the SA algorithm, each network of m sensors is considered as a state of a virtual physical system, and the objective function is interpreted as the internal energy of this system in a given state. According to statistical thermodynamics, the probability of a physical system being in a state β follows the Boltzmann distribution

$$P_\beta = \frac{1}{Z}\exp\left(-\frac{\Delta E_\beta}{K_\beta T}\right),$$

where Z is the partition function, E_β is the internal energy, T is the temperature at the state β, and K_β is the Boltzmann constant. Using an analogy, during the minimization process in SA, the probabilistic treatment consists of accepting a new network selected in the neighbourhood of the current network following the probability $P = \exp(-\Delta J/T)$, where ΔJ is the cost difference between the new and the current configurations. At high temperature, the SA performs a coarse search of the space of global states, avoids local minima and finds a good minimum. As the temperature is lowered, the search becomes fine in the neighbourhood of the already determined minimum and the SA reaches a better minimum. It is useful to note that there is no certainty in convergence of the SA (Cohn and Fielding, 1999), however it is likely that a "near-optimal" network configuration can be reached (Altinel *et al.*, 2008).

Implementation of SA requires a careful parametrization operation. The best cooling schedule (i.e. the temperature decay law) follows the Exponential Cooling Scheme (ECS; Nourani and Andresen, 1998) as $T_{i+1} = \theta T_i$, where T_i and T_{i+1} and are respectively the temperatures at iterations i and $i+1$. Here, θ is often named as the decay factor and it determines the cooling rate (i.e. the convergence rate of the SA). It is therefore important that this value be close to 1 for giving time to the algorithm to exploring a large search space and to avoid a premature convergence to a local minimum (Kirkpatrick *et al.*, 1983; Abida *et al.*, 2008; Siarry, 2014; Du and Swamy, 2016). To give more chance to converge to the global optimum, a large number of iterations at each temperature must be performed (Hajek, 1987). A proposition for the number of iterations at a given temperature level is given in Siarry (2014). The initial temperature T_0 can be fixed for acceptance probability P_0 of about 0.8 as suggested by Kirkpatrick *et al.* (1983). T_0 clearly depends on the scaling of S_ϕ, therefore it can be fixed by conducting an initial search for a sample of random network configurations. A suggestion for the sample size of the random network configurations was described in Siarry (2014). T_0 is obtained by the Metropolis law:

$$T_0 = -\frac{\overline{\Delta S_\phi}}{\log(P_0)},$$

where $\overline{\Delta S_\phi}$ is an average of the difference of cost functions calculated for a large number of cases. For fixing the stopping temperature T_{stop}, no general rule is available. Therefore, calculation can be stopped when no improvement in the cost function is observed.

3 | SOURCE RECONSTRUCTION APPROACH

In order to validate the performance of the optimal networks obtained from the described methodology in section 2, the renormalization inversion approach coupled with a CFD modelling approach (Sharan *et al.*, 2009; Kumar *et al.*, 2015b) is utilized to estimate an unknown continuous point release in an urban environment. The methodology is briefly described as follows.

3.1 | Renormalization inversion theory

The renormalization approach is based on a linear source–receptor relationship that describes the effect of a polluting source of a given strength at one location on the species concentrations at the receptors at different locations (Marchuk, 1995). In the case of a continuous release of the passive tracer, the concentration measurement μ_i, sampled by the ith detector can be modelled by:

$$\mu_i = \int_\Omega s(\mathbf{x}) a_i(\mathbf{x})\, \mathrm{d}\mathbf{x}, \tag{7}$$

where $s(\mathbf{x})$ is the source function that represents the rate of contaminant release per unit area and time.To solve the inverse problem is to estimate the source $s(\mathbf{x})$ from Equation 7. This problem is ill-posed and has an infinite number of solutions (i.e. the unknown number is greater than the number of measurements). In order to obtain a unique solution, Sharan *et al.* (2009) proposed a decomposition $s(\mathbf{x}) = s_\parallel(\mathbf{x}) + s_\perp(\mathbf{x})$ of the source function $s(\mathbf{x})$ into two components which are parallel ($s_\parallel$) and orthogonal ($s_\perp$) to the adjoint fields. The orthogonal component $s_\perp(\mathbf{x})$ verifies $\langle s_\perp(\mathbf{x}), a_i(\mathbf{x})\rangle = 0$, and does not contribute in the reconstruction of the measurements. Thus, only the observable parallel component $s_\parallel(\mathbf{x})$ to the adjoint fields is considered. Therefore, if the concentration measurements $\boldsymbol{\mu} = (\mu_1, \mu_2, ..., \mu_m)^{\mathrm{T}} \in \mathbf{R}^m$ are available from m sensors, a solution to the inverse problem can be formulated as (Sharan *et al.*, 2009)

$$s_\parallel(\mathbf{x}) = \mathbf{a}^{\mathrm{T}}(\mathbf{x})\mathbf{H}^{-1}\boldsymbol{\mu}, \tag{8}$$

where $\mathbf{H}$ is the Gram matrix with elements $H_{ij} = \int_\Omega a_i(\mathbf{x}) a_j(\mathbf{x})\, \mathrm{d}\mathbf{x}$.

Issartel (2005) showed that the source estimated from Equation 8 is concentrated at the sensors' locations and justified this property by the singular values of the retroplumes close to the sensors. In order to eliminate the singularities at the detector locations and to minimize the inversion artifacts, the renormalization theory was proposed and justified by Issartel (2005). The renormalization approach is based on the introduction of a renormalized weight function $f(\mathbf{x})$ and accordingly, Equation 7 becomes

$$\mu_i = \int_\Omega s(\mathbf{x}) a_{fi}(\mathbf{x}) f(\mathbf{x})\, \mathrm{d}\mathbf{x}. \tag{9}$$

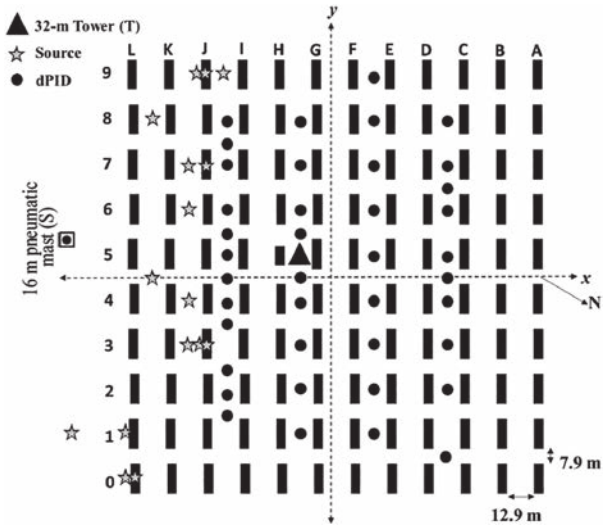

FIGURE 1 A schematic diagram of the MUST geometry showing 120 containers and source (stars) and receptor (black filled circles) locations. In a given trial, only one source was operational

Accordingly, the new estimated source function (Equation 8) is given by

$$s_{\parallel f}(\mathbf{x}) = \mathbf{a}_f^{\mathrm{T}}(\mathbf{x})\mathbf{H}_f^{-1}\boldsymbol{\mu}, \tag{10}$$

where $\mathbf{a}_f$ and $\mathbf{H}_f^{-1}$ were defined in section 2.1. The visibility function $\phi(\mathbf{x})$ (i.e. converged value of $f(\mathbf{x})$) was calculated using the iterative algorithm described in Equation 3. Then, the source estimate function $s_{\parallel\phi}(\mathbf{x})$ is calculated with this converged value $\phi(\mathbf{x})$ of $f(\mathbf{x})$.

3.2 | Point source estimation

The renormalization theory allows estimation of distributed and point releases. For distributed source, the estimation of $s_{\parallel\phi}(\mathbf{x})$ is defined at every point of the domain and, as a particular case, the maximum of the estimation, i.e. $\max(s_{\parallel\phi}(\mathbf{x}))$, corresponds to the location of a point source. Indeed, for a point release from $\mathbf{x}_0$ with intensity Q_0, the source can be expressed by $s(\mathbf{x}) = Q_0\delta(\mathbf{x}-\mathbf{x}_0)$ and associated ideal measurements by $\boldsymbol{\mu} = Q_0\mathbf{a}(\mathbf{x}_0)\phi(\mathbf{x}_0)$ (from Equation 9). By replacing the measurement term in Equation 10, the estimation of a point source can be obtained as

$$s_{\parallel\phi}(\mathbf{x}) = Q_0\phi(\mathbf{x}_0)\mathbf{a}_\phi^{\mathrm{T}}(\mathbf{x})\mathbf{H}_\phi^{-1}\mathbf{a}_\phi(\mathbf{x}_0). \tag{11}$$

Using the Cauchy–Schwartz inequality and the renormalization condition (iii) (Equation 3) in Equation 11, $s_{\parallel\phi}(\mathbf{x})$ reaches its maximum only at a position $\mathbf{x} = \mathbf{x}_0$ and thus, the intensity is obtained as

$$Q_0 = s_{\parallel\phi}(\mathbf{x}_0)/\phi(\mathbf{x}_0). \tag{12}$$

4 | MOCK URBAN SETTING TEST (MUST) FIELD EXPERIMENT

In the framework of the Mock Urban Setting Test (MUST; Biltoft, 2001), a standard urban network was formed in order

TABLE 1 Source details and meteorological conditions in 20 selected trials of the MUST field experiment (Biltoft, 2001; Yee and Biltoft, 2004)

Trial no.	Trial name (JJJhhmm)	q_s (l/min)	t_s (min)	z_s (m)	S_{04} (m/s)	α_{04} (deg)	u_* (m/s)	L (m)	k (m^2/s^2)
1	2640138	175	21	0.15	2.35	17	0.26	91	0.359
2	2640246	200	15	0.15	2.01	30	0.25	62	0.306
3	2671852	200	22	0.15	3.06	−49	0.32	330	0.436
4	2671934	200	15	1.8	1.63	−48	0.08	5.8	0.148
5	2672033	200	15	1.8	2.69	−26	0.17	4.8	0.251
6	2672101	200	14	0.15	1.89	−10	0.16	7.7	0.218
7	2672150	200	16	0.15	2.30	36	0.35	150	0.409
8	2672213	200	15	1.8	2.68	30	0.35	150	0.428
9	2672235	200	15	2.6	2.32	36	0.26	48	0.387
10	2672303	200	19	1.8	2.56	17	0.25	74	0.367
11	2681829	225	15	1.8	7.93	−41	1.10	28000	1.46
12	2681849	225	16	0.15	7.26	−50	0.76	2500	0.877
13	2682256	225	15	0.15	5.02	−42	0.66	240	0.877
14	2682320	225	15	2.6	4.55	−39	0.50	170	0.718
15	2682353	225	15	5.2	4.49	−47	0.44	120	0.727
16	2692054	225	22	1.3	3.34	39	0.36	170	0.362
17	2692131	225	17	1.3	4.00	39	0.42	220	0.582
18	2692157	225	15	2.6	2.98	43	0.39	130	0.505
19	2692223	225	15	1.3	2.63	26	0.35	120	0.484
20	2692250	225	17	1.3	3.38	36	0.37	130	0.537

Here, Trial nos. 1–20 are assigned for simplicity and do not correspond to original assigned trial numbers in the MUST experiment.
Source parameters are release rate q_s, release duration t_s, and source height z_s.
S_{04} and α_{04} are wind speed and direction at the 4 m level at mast S.
u_*, L and k are the friction velocity, Obukhov length and turbulent kinetic energy at the 4 m level at tower T.

to improve the characterization of plume transport and dispersion around buildings. This field campaign was organized by the Defense Threat Reduction Agency (DTRA) and was conducted in September 2001 at Dugway Proving Ground in western Utah, USA. The experiment presented a comprehensive dataset for the modellers and provided an opportunity for fine analysis of the physical transport mechanisms around the urban canopy. The MUST experiment consisted of releases of the propylene gas (C_3H_6) into the atmosphere. The dispersion of the released gas was measured in an idealized urban geometry of dimensions 200×200 m^2. The urban canopy is represented by a grid of containers arranged in 10 rows and 12 columns on the ground surface as shown in Figure 1. Each container has dimensions 2.54 m height, 12.2 m length and 2.42 m width. The spacing between the lines is 12.9 m and the columns are separated by a distance of 7.9 m. In this study, 20 trials of continuous releases under stable and neutral meteorological conditions are considered. For these trials, the sources were located at different positions inside and outside the canopy and at different heights above the ground surface (Biltoft, 2001).

In a given trial of the MUST experiment, the gas was continuously released over ≈15 min and concentration measurements were made using a standard network of 48 photoionization detectors (PIDs). Forty sensors were positioned on four horizontal lines at 1.6 m height above the ground surface and eight additional detectors were placed at various altitudes (from 1 to 16 m) approximately at the centre of the domain. For characterizing the wind and turbulence, eight anemometers were distributed on four masts at different altitudes. The values of the meteorological and turbulence variables and source parameters in all selected trials are taken from Biltoft (2001) and Yee and Biltoft (2004) and presented in Table 1.

5 | CFD ADJOINT FIELDS

In a study by Kumar *et al.* (2015b), which aimed to couple and evaluate the renormalization method with a CFD modelling approach for the reconstruction of a continuous point source in an urban environment, a CFD model fluidyn-PANACHE (Fluidyn-Panache, 2010) was used to calculate the retroplumes. These retroplumes were calculated for the standard network of 40 sensors deployed at 1.6 m above the ground surface in each trial of the MUST field experiment. This CFD model is able to represent the geometric and flow complexity inherent in the urban regions. The computation of the retroplumes was performed in two steps. In the first step, simulations of the CFD model for the converged flow-fields in each trial were performed by solving the three-dimensional (3D) Reynolds-averaged Navier–Stokes equations using a

finite-volume numerical scheme. Secondly, the flow-field was reversed (i.e. the direction of the computed steady state flow field is reversed 180∘ by simply changing the wind field sign) and used in the standard advection–diffusion equation to compute the retroplumes. A receptor is considered as a virtual point source of unit strength in the advection–diffusion equation for computation of a retroplume.

For CFD simulations and other calculations, the computation domain was decomposed into two domains: the inner domain is defined (250 m × 225 m × 100 m) to refine meshes around the obstacles, and an outer one (800 m × 800 m × 200 m) was defined to have a smooth flow at the inner domain boundary and also to reduce the direct effect of inflow boundary conditions imposed at the inlet of the outer domain. A 3D unstructured mesh was generated in both domains. The mesh was further refined near the obstacles and at locations of the receptors. Both outer and inner computational domains were discretized respectively in 61 and 56 vertical levels with minimum vertical grid spacing of 0.25 m near the ground surface. The lowest 40 vertical levels in both domains were set to a uniform 0.25 m grid spacing to cover the lowest 10 m (approximately four times the obstacle height of 2.54 m) of the vertical domains. The computational domain contains a total of 2,849,276 grid cells in the embedded mesh. A grid sensitivity analysis with other mesh resolutions was also performed to adapt the defined mesh for the numerical simulation. A two-equation k–ϵ turbulence model was used derived from the standard high-Reynolds-number (Re) form with corrections for buoyancy and compressibility (Launder, 2004; Hanjalic, 2005). The details about the inflow profiles (wind, temperature and turbulence), the prediction errors of the forward CFD model, the duality verification, and the sources reconstruction using the original network, are available in Kumar *et al.* (2015a; 2015b) . The boundary conditions are now briefly presented.

Based on the direction of the mean wind with respect to the domain boundary, the lateral boundaries of the computational domain were considered as inflow and outflow boundaries. The top boundary was treated as an outflow boundary. The bottom boundary condition at the ground surface was defined by a no-slip condition. Standard wall functions (Hanjalic, 2005) were used to compute the drag forces on solid walls in a turbulent boundary layer. The velocity, temperature, and turbulence variables at the inflow boundary were specified as follows:

1. *Wind profile*. The wind profiles proposed by Gryning *et al.* (2007) in stable and neutral conditions were used for inflow condition which are applicable in the entire atmospheric boundary layer (ABL) and are composed of the three different length-scales in surface, middle, and upper layers of the ABL. As the Gryning *et al.* (2007) wind profile is not suitable for very stable atmospheric conditions, a wind profile based on a similarity function proposed by Beljaars and Holtslag (1991) and applicable for extremely stable conditions (Sharan and Kumar, 2010) was used.
2. *Temperature profile*. The logarithmic temperature profile based on the Monin–Obukhov similarity theory was used to describe the temperature vertical variation in neutral and stable conditions.
3. *Turbulence profiles*. The profiles of k and ϵ based on an approximate analytical solution of the one-dimensional k–ϵ prognostic equation (Yang *et al.*, 2009) were used for inflow boundary conditions. Coefficients in these profiles of k and ϵ are estimated based on the observations of k.

6 | DESCRIPTION OF THE NUMERICAL COMPUTATIONS

For the optimal design of the sensor networks in an urban environment by the methodology described above, the calculations were performed by coupling (a) the renormalization inversion algorithm, (b) the stochastic algorithm (SA) and (iii) the CFD adjoint fields. The objective is to find the best set of $m = 10$ and 13 among the $p = 40$ potential locations (standard network) in order to reconstruct the sources in 20 selected trials of the MUST field experiment. For this study, the numbers of sensors were not fixed arbitrarily. In fact, it was observed that an acceptable estimation of the source in the majority of the trials was enabled by using a minimum of eight sensors in the defined domain (Kouichi, 2017). Also, using more than 13 sensors in an optimal network, the errors in source parameter estimation are stable and do not improve significantly. For this reason, the optimal network designs were constructed and evaluated for sizes $m = 10$ and 13 (one quarter and one third of the original network of 40 sensors).

The calculations can be described by following three main steps:

1. For a given initial network and the meteorological conditions in each trial of the MUST experiment, the converged flow-field and then the adjoint fields were calculated (at one time for all the sensors) using the CFD model fluidyn-PANACHE (Fluidyn-Panache, 2010). The meteorological and turbulence variables to simulate the flow-field by fluidyn-PANACHE includes (a) wind speed and direction, (b) temperature, (c) friction velocity, (d) surface heat flux, and (e) turbulent kinetic energy. The measurements of these meteorological and turbulence variables were also used to specify the inflow boundary conditions. A retroplume was calculated by reversing the wind direction and considering a sensor as a virtual point source of unit intensity. The obtained retroplumes that represent the sensitivity of the sensors in the computational domain were archived as new data files.
2. When the archived retroplumes for a MUST trial were available from Step 1, the optimization process was

performed. The parameters of the SA algorithm were set according to their properties described in section 2.2. The implemented algorithm follows a decay by level (i.e. the temperature remains constant in each level for L_T iterations). Before starting the iterative process, a first network N_{best} was randomly selected in the search space I (Equation 5). Considering the sensor locations of N_{best}, the optimal weighting function $\phi(\mathbf{x})$ and $\mathbf{H}_\phi$ (Equations 3 and 4) were computed iteratively and then the entropy $S_\phi(N_{\text{best}})$ (Equation 5). In these computations, firstly the renormalization algorithm was used to compute $\phi(\mathbf{x})$ iteratively (Equation 1) and the optimal weighted Gram matrix $\mathbf{H}_\phi$ (Equation 2). The calculation of the renormalized weights required about 20 iterations in the renormalization algorithm. Then the cost function $S_\phi(N_{\text{best}})$ was calculated from Equation 5. It is interesting to note that N_{best} corresponds to a set of $m = 10$ or $m = 13$ sensors for the MUST experiment's network. For each temperature level, L_T iterations were performed during which a new network (N_{new}) was randomly selected and the following operations iteratively repeated:

Compute the entropy $S_\phi(N_{\text{new}})$ and the difference $\Delta S_\phi = S_\phi(N_{\text{best}}) - S_\phi(N_{\text{new}})$.

(a) if $\Delta S_\phi < 0$, the entropy has increased and N_{new} becomes N_{best}.

(b) if the entropy decreases ($\Delta S_\phi > 0$), but crosses the acceptance probability ($P \leq \exp(-\Delta S_\phi/T)$), N_{new} is nevertheless retained and becomes N_{best}, so the SA can avoid local maxima.

After L_T iterations, the temperature was lowered until the stop temperature T_{stop} was reached.

3. At the stop temperature, the N_{best} network became the optimal network N^{o} containing the maximum information. The source term parameters were then calculated using the renormalization inversion algorithm (Equations 11 and 12)

This process of the optimization was performed iteratively and stochastically according to the SA algorithm until the optimal network N^{o} that verified the conditions (a) and (b) described in Equation 6 were obtained. The parameters for SA were chosen carefully according to the literature recommendations, the scale of the cost function S_ϕ and according to the number of possible combinations C_m^p. Setting parameters for the SA algorithm are given in Table 2. The optimization calculations were performed on a computer of characteristics: Intel® Core™ i7-4790 CPU @ 3.60 GHz and 16 GB RAM. The average time elapsed in the optimization of one network for a single trial was ≈ 2.5 hr for 10 sensors and ≈ 8.5 hr for 13 sensors.

TABLE 2 Setting parameters for the SA algorithm

m	T_0	T_{stop}	L_T	θ	N_C
10	15	10^{-11}	100	0.9	8.5×10^8
13	15	10^{-11}	200	0.9	1.2×10^{10}

T_0 and T_{stop} are respectively the initial and final temperatures, L_T is the number of iterations performed at a temperature level T, θ is the decay factor, N_C is the number of possible combinations and m is the detector number.

7 | RESULTS AND DISCUSSIONS

The coupling of the renormalization algorithm, the CFD adjoint fields and the optimization algorithm SA was successfully achieved and the optimal networks of 10 and 13 sensors were obtained for all 20 trials of the MUST field experiment. Representative results of the optimal networks of 10 and 13 sensors and their corresponding source estimation results in the form of contour plots of the visibility function $\phi(\mathbf{x})$ and the normalized source estimate function $\mathbf{s}^{\text{n}}_{\|\phi}(\mathbf{x}) = \mathbf{s}_{\|\phi}(\mathbf{x}) / \max(\mathbf{s}_{\|\phi}(\mathbf{x}))$ are shown in Figures 2 and 3 for different MUST tracer releases by source position in trials 3 (Wide Alley), 7 (Upwind Face), 10 (Intersection), 15 (Conex Roof), and 20 (Outside Array). The source reconstruction in each trial was performed by taking the measurements only from the sensors in the optimal networks. The optimal networks of sizes $m = 10$ and $m = 13$ for all selected 20 MUST trials are shown in Supporting Information Figures S1.1 and S1.2 and the respective isopleths of the renormalized weight function $\phi(\mathbf{x})$ and the normalized source estimate function $\mathbf{s}^{\text{n}}_{\|\phi}(\mathbf{x}) = \mathbf{s}_{\|\phi}(\mathbf{x}) / \max(\mathbf{s}_{\|\phi}(\mathbf{x}))$ are shown in Figure S2.

The first analysis concerns the optimal network structures in the urban space of the MUST experiment. Qualitatively, a widely dispersed distribution of the sensors was noted for all network sizes and for all selected MUST trials. This shows that for a given wind direction (opposite direction to the visibility fields orientation), no specific region in the monitored area is privileged. In this distribution, a larger area is covered by significantly higher values of the visibility function. Accordingly, it allows us to monitor an important region for the source reconstruction. In isopleths of the visibility functions (Figures 2, 3 and S2), the unseen regions are represented by black, whereas the zones seen by the optimal network are illustrated by white and grey shades.

In order to evaluate the performance of the optimal networks based on the entropic criterion, the source reconstructions were first compared with results computed from the original MUST network formed by 40 sensors. This comparison study permits us to analyze the impact of the reduction of the size of the original network in various meteorological and source conditions. Secondly, the performances of the optimal networks based on the entropic criterion were also compared with source reconstruction results computed from the optimal networks based on the normalized errors between the modelled and observed concentration measurements (Kouichi *et al.*, 2018). This permits us to analyze the efficiency of the optimal networks design at local scale in an urban domain based on *a priori* information of the source (i.e. using the measurements from a specific source) and based on the characteristics of the networks without any prior information of the source (i.e. using the information contained in a network from the present entropic criterion).

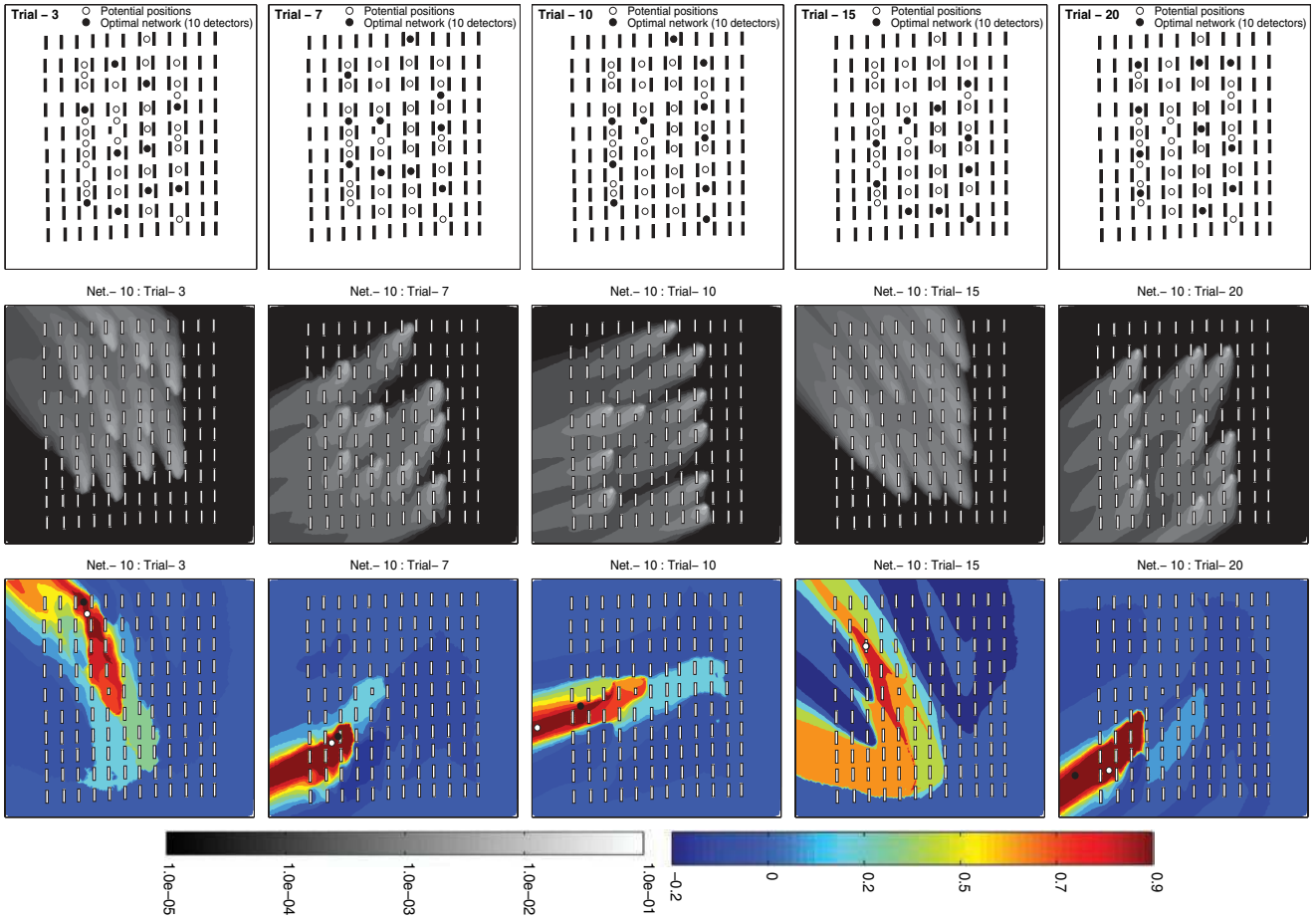

FIGURE 2 The 10-sensor optimal networks (first row), corresponding contour plots of the visibility function $\phi(\mathbf{x})$ (second row) and the normalized source estimate function $\mathbf{s}^{\mathrm{n}}_{\|\phi}(\mathbf{x}) = \mathbf{s}_{\|\phi}(\mathbf{x}) / \max(\mathbf{s}_{\|\phi}(\mathbf{x}))$ (third row) for different MUST tracer releases by position in trials (from left to right) 3 (Wide Alley), 7 (Upwind Face), 10 (Intersection), 15 (Conex Roof), and 20 (Outside Array). The black and white filled circles in the third row respectively represent the true and estimated source locations

7.1 | Optimal design by reduction of an original network size

Source estimation results from the different optimal networks are shown in Table 3 for all 20 trials of the MUST experiment and the respective isopleths of the normalized source estimate function $\mathbf{s}^{\mathrm{n}}_{\|\phi}(\mathbf{x})$ are shown in Figure S2. These results are presented in terms of the location error (E_l), which is the Euclidean distance between the estimated and the true source locations, and (E_q) a ratio of the estimated to true source intensity. The networks are presented by the superscript m representing the sizes of a network (i.e. number of sensors) on E_l^m and E_q^m.

Using the measurements from the original network of 40 sensors in all 20 trials, the location error varies from 1.10 to 42.90 m (Table 3). This give rises to an average location error of 14.62 m for all 20 trials. Note that these location errors occur in a 200 m × 200 m computational domain of the MUST field experiment. The source intensities were estimated between an overestimation by a factor of 4.01 and an underestimation of 0.27. In 75% of the trials, source intensities were estimated within a factor of two to the true release rate.

Using the concentration measurements from the optimal networks of 13 sensors in each MUST trial, the location errors were estimated between 3.84 m (trial 6) and 48.62 m (trial 3) and the average location error for all 20 trials was 21.49 m (Table 3). Concerning E_q^{13}, ratios of the estimated to the true source release rates varied between 0.63 and 2.15 (Table 3). In 80% of the trials, the source intensity was estimated within a factor of two to the true release rates, and a consistent estimation of these intensities was observed from these networks of 13 sensors.

Using the concentration measurements from the optimal networks of 10 sensors, the best estimation of the source location was 0.36 m (trial 15) and largest error observed was 47.63 m in trial 10 (Table 3). For all 20 trials, the average location error was 18 m. For these optimal networks, E_q^{10} varied from 0.84 (trial 20) to 2.37 (trial 10) (Table 3) and in 70% of the trials, it was estimated within a factor of two of the true release rate. It was also observed that the estimated release rates in all 20 trials were within a factor of 2.37 and no unusual over/underestimation was observed from these optimal networks (Table 3). This shows a consistent estimation of the unknown source intensities from the optimal networks of 10 sensors.

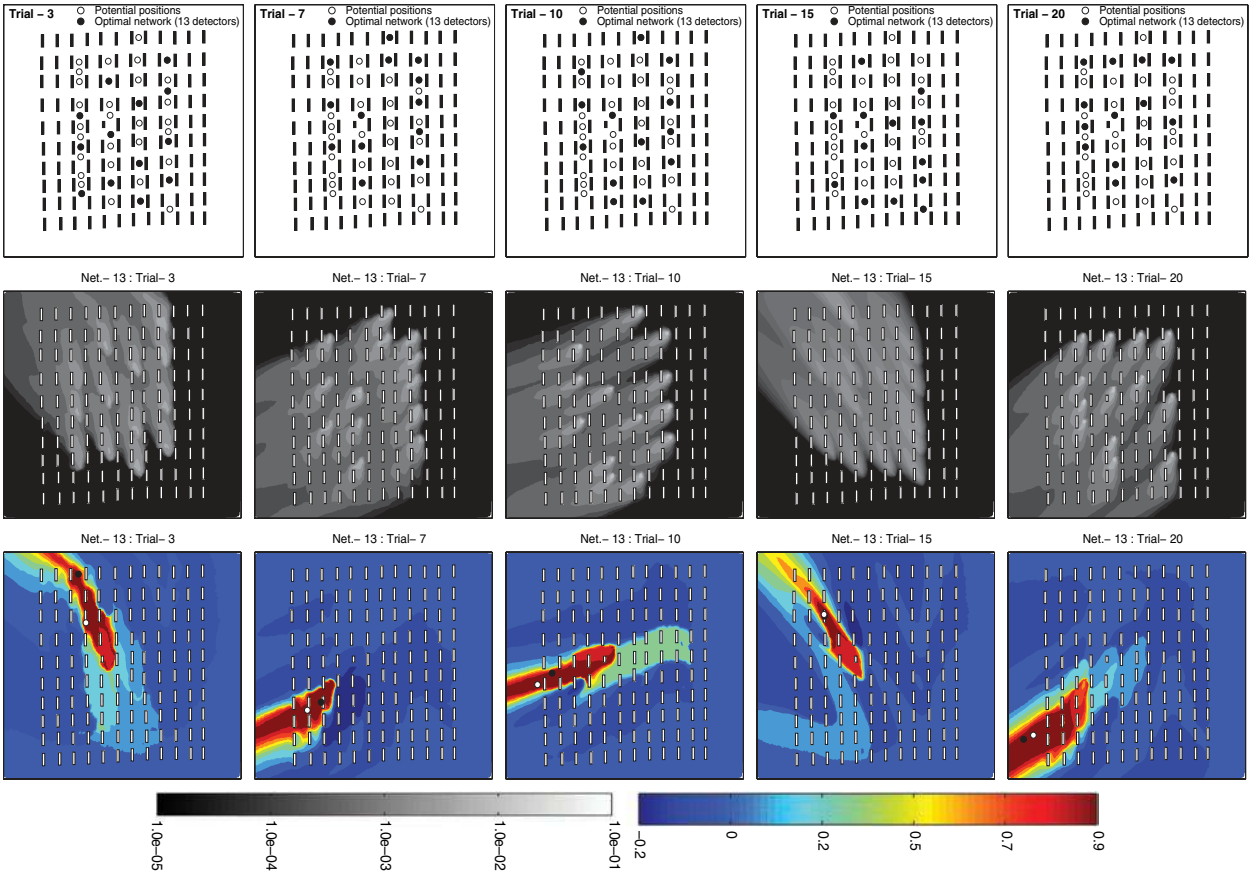

FIGURE 3 As Figure 2, but for the 13-sensor optimal networks

From this quantitative analysis, it seems that the optimal design based on the entropic criterion leads to the acceptable optimal networks to estimate an unknown release in an urban-like environment. The reduction in the number of sensors from the original network to one quarter and one third does not significantly degrade the performance of the source term estimation. Also, the performance of the optimal networks is comparable to the original network in the majority of the trials. The precision in source parameter reconstruction is also improved by using the information from optimal networks in some of the trials.

7.2 | Performance comparison of the optimal networks with and without *a priori* source information

Recently, Kouichi *et al.* (2018) described a methodology for the optimal design of a monitoring network based on *a priori* information of the source by using the concentration measurements in the optimization process. However, designing the optimal monitoring networks in this study is purely based on available knowledge of meteorological conditions and does not require any information of the pollutant source and the associated concentrations at the receptors. Thus, the efficiency of the present methodology for optimization without *a priori* information of the source and concentration measurements was compared with the optimal networks designed with *a priori* measurements being used in the optimization process. The performance of optimal networks ($m = 10$ and 13) based on the entropic criterion is compared with performance of optimal networks based on the normalized errors presented in Kouichi *et al.* (2018). Source estimation results for the different optimal networks from both approaches are shown in Table 3 for all 20 trials in the MUST field experiment.

It was observed that the performance of the present optimal networks in terms of source estimation are comparable with those based on the normalized errors (Table 3). Using 10 and 13 sensors, the averaged location errors estimated from the optimal networks from the entropic criterion for all 20 trials are respectively 18 and 21.48 m. However, these averaged location errors from optimal network of normalized errors were 19.20 and 17.42 m respectively for 10 and 13 sensors networks. In term of the estimation of the source intensity, new optimal networks from the entropic criterion also have comparable performances with Kouichi *et al.* (2018). Using the measurements from 10- and 13-sensor optimal networks, the present optimal networks from the entropic criterion estimated the source intensities within a factor of two in 70 and 80% of the trials which is also comparable with 80% of the trials from the optimal networks from the method of normalized errors (Table 3). The results in Table 3 also show that the concept of information (quantified by the entropic criterion) in optimal design of the monitoring networks is a fine concept

TABLE 3 Source estimation results from the different monitoring networks of 10 and 13 sensors for each MUST trial

	Original network		**Entropic criterion**				**Normalized Error criterion**			
Trial no.	E_l^{40} **(m)**	E_q^{40}	E_l^{13} **(m)**	E_l^{10} (m)	E_q^{13}	E_q^{10}	E_l^{13} **(m)**	E_l^{10} **(m)**	E_q^{13}	E_q^{10}
1	3.30±(1.30)	0.92±(0.08)	17.67±(7.23)(7.49)(8.21)	4.00±(0.29)(1.62)(1.67)	1.10±(0.09)(0.10)(0.12)	1.05±(0.07)(0.12)(0.13)	19.60±(12.13)	33.76±(5.30)	1.04±(0.23)	1.24±(0.22)
2	42.90±(23.80)	4.01±(1.57)	5.87±(0.86)(9.05)(12.52)	24.09±(4.48)(6.08)(11.08)	1.61±(0.05)(0.38)(0.50)	2.08±(0.10)(0.15)(0.22)	31.91±(8.80)	56.88±(9.51)	3.21±(0.41)	5.12±(3.63)
3	10.80±(1.60)	1.17±(0.27)	48.62±(12.98)(14.17)(16.28)	15.86±(1.47)(1.65)(6.73)	0.91±(0.04)(0.05)(0.07)	0.91±(0.04)(0.05)(0.08)	9.01±(2.47)	9.01±(3.02)	0.71±(0.16)	0.71±(0.16)
4	22.80±(7.70)	0.27±(0.35)	33.93±(0.00)(0.31)(0.87)	26.97±(3.02)(3.16)(3.78)	2.15±(0.08)(0.10)(0.14)	2.20±(0.13)(0.16)(0.19)	18.07±(1.84)	18.07±(2.61)	0.83±(0.21)	0.83±(0.26)
5	21.90±(2.10)	0.57±(0.07)	21.88±(3.20)(4.11)(5.03)	11.33±(1.16)(2.17)(3.09)	0.63±(0.29)(0.29)(0.33)	1.69±(0.10)(0.15)(0.19)	2.13±(2.54)	11.56±(4.21)	0.95±(0.05)	0.67±(0.05)
6	5.00±(1.60)	2.14±(0.60)	3.84±(1.81)(2.03)(2.81)	11.65±(2.88)(3.68)(4.37)	2.10±(0.13)(0.17)(0.21)	1.78±(0.08)(0.12)(0.18)	6.96±(0.19)	6.96±(0.00)	1.04±(0.06)	1.04±(0.04)
7	12.40±(9.10)	0.41±(0.49)	16.39±(3.24)(4.18)(4.57)	8.78±(3.55)(4.42)(5.07)	1.88±(0.13)(0.21)(0.22)	1.72±(0.09)(0.13)(0.16)	18.85±(9.08)	12.99±(1.67)	3.11±(0.51)	1.06±(0.07)
8	15.80±(12.10)	2.22±(0.90)	20.58±(10.06)(10.19)(10.75)	12.82±(2.44)(3.11)(4.69)	1.59±(0.36)(0.35)(0.34)	1.57±(0.07)(0.10)(0.14)	12.86±(1.28)	15.79±(1.05)	1.32±(0.34)	1.76±(0.11)
9	7.70±(1.20)	1.37±(0.07)	6.89±(0.55)(0.83)(1.17)	12.16±(0.75)(1.13)(1.26)	1.93±(0.07)(0.10)(0.12)	1.11±(0.13)(0.26)(0.33)	8.20±(0.35)	8.08±(0.00)	3.06±(0.17)	7.55±(0.39)
10	8.80±(3.00)	1.08±(0.19)	31.90±(7.50)(8.53)(8.73)	47.63±(5.50)(7.69)(9.63)	2.07±(0.25)(0.39)(0.42)	2.37±(0.15)(0.18)(0.21)	8.00±(4.57)	8.00±(0.00)	1.08±(0.77)	1.08±(1.07)
11	19.80±(5.00)	1.67±(0.12)	36.60±(6.65)(8.78)(11.19)	34.64±(9.01)(11.57)(15.74)	2.15±(0.13)(0.15)(0.18)	2.11±(0.20)(0.24)(0.32)	17.19±(12.00)	17.19±(7.06)	1.62±(0.40)	1.62±(0.26)
12	7.40±(6.60)	0.95±(0.06)	29.47±(4.63)(8.60)(11.06)	22.55±(19.07)(19.12)(19.32)	1.46±(0.11)(0.15)(0.19)	1.27±(0.11)(0.13)(0.17)	5.43±(11.69)	10.22±(9.10)	0.85±(0.28)	0.20±(0.04)
13	7.70±(0.60)	0.97±(0.07)	6.64±(0.19)(0.65)(0.89)	11.46±(6.93)(7.77)(9.14)	1.70±(0.07)(0.11)(0.14)	1.66±(0.09)(0.10)(0.13)	8.63±(4.36)	8.63±(3.86)	0.78±(0.18)	0.78±(2.05)
14	2.20±(1.90)	1.42±(0.17)	21.80±(11.60)(13.45)(14.15)	38.75±(2.83)(7.25)(8.21)	1.57±(0.16)(0.18)(0.22)	2.25±(0.07)(0.19)(0.23)	5.50±(2.98)	5.50±(3.88)	0.88±(0.24)	0.88±(0.40)
15	1.10±(1.00)	1.88±(0.09)	1.62±(0.93)(3.17)(3.97)	0.36±(0.74)(3.25)(3.63)	1.52±(0.05)(0.09)(0.11)	2.11±(0.01)(0.11)(0.13)	30.23±(2.14)	37.98±(0.72)	0.57±(0.07)	0.17±(0.01)
16	26.70±(4.90)	1.70±(0.06)	23.96±(1.82)(2.17)(2.98)	23.96±(0.23)(1.16)(6.10)	1.48±(0.04)(0.07)(0.09)	1.44±(0.08)(0.09)(0.13)	63.04±(6.84)	29.80±(9.86)	0.29±(0.06)	0.67±(0.23)
17	7.00±(1.90)	0.90±(0.05)	40.50±(4.16)(4.39)(4.40)	6.21±(1.56)(2.00)(3.45)	1.34±(0.05)(0.07)(0.08)	1.21±(0.06)(0.08)(0.11)	14.07±(2.78)	23.05±(10.44)	1.10±(0.04)	1.52±(0.16)
18	14.30±(11.00)	1.15±(0.46)	22.01±(2.72)(4.17)(7.30)	6.98±(0.98)(1.63)(2.63)	0.92±(0.06)(0.08)(0.12)	1.22±(0.08)(0.08)(0.11)	12.83±(4.18)	12.83±(4.61)	1.15±(0.16)	1.15±(0.21)
19	22.30±(6.40)	1.76±(0.16)	14.25±(11.94)(12.66)(13.80)	5.26±(7.93)(8.87)(9.72)	1.67±(0.16)(0.19)(0.23)	1.77±(0.23)(0.24)(0.26)	10.77±(4.25)	13.46±(4.80)	0.99±(0.20)	0.83±(0.25)
20	35.50±(1.80)	0.83±(0.04)	25.31±(10.80)(11.24)(11.33)	34.64±(1.24)(1.93)(5.47)	0.97±(0.18)(0.19)(0.21)	0.84±(0.03)(0.04)(0.08)	45.23±(1.78)	44.29±(0.31)	1.68±(0.06)	1.56±(0.06)

E_l^p and E_q^p respectively denote the location error (m) and ratio of the estimated to true source intensity with the corresponding monitoring network. Here, the superscript p on E_l^p & E_q^p represents the number of sensors in an optimal network. For comparison, source estimation results for the original network and the optimal networks from the Normalized Error criterion are taken from Kumar *et al.* (2015b) and Kouichi *et al.* (2018), respectively. The (first) parentheses give the standard deviations of the estimated source parameters with 10% noise in the measurements. Values in second and third parentheses in the Entropic criterion columns are the standard deviations with 15 and 20% respectively added noise in the measurements.

since, in most of the trials, increasing the number of sensors improved the estimation of source parameters. However, this is not observed in some MUST trials using the normalized errors. It is also noted that the estimated intensities from the present optimal networks are more consistent than the normalized errors criterion over all the trials. The estimated source intensities were not as consistent in some trials in Kouichi *et al.* (2018); for example, in the 10-sensor networks, the source intensities in trials 2 and 9 were highly overestimated by factors of 5.12 and 7.55, respectively (Table 3). A great advantage of the present methodology is that the optimization of the sensor networks does not require *a priori* information of the source which was essential in the optimization methodology of Kouichi *et al.* (2018).

In order to evaluate the stabilties of the estimation of the source parameters using the optimal networks, posterior uncertainties on the source position and intensity are calculated due to measurements errors. The renormalization inversion technique does not require computation of the weight function with the noisy measurements because the computation of the weight function is independent of the concentration measurements. For quantifying the uncertainty, a 10% Gaussian noise was added at each measurement. Using the obtained optimal networks, 50 simulations for the source reconstruction were performed for each trial. The average and the standard deviation of E_q and E_l were calculated and the results presented in Table 3. For the optimal networks, there is not an obvious trend and the uncertainties are in the same order of magnitude as the original network (40 sensors) and the optimal networks obtained based on the normalized errors cost function. As 10% noise is rather a low value to analyze the uncertainties, some additional computations were also performed by adding 15 and 20% random error on the observations. The results based on these computations with 15 and 20% are included in Table 3. From these values in Table 3, it can be observed that the uncertainties in the estimated source parameters increase with the increasing noise on the measurements.

It is also useful to test how the renormalization inversion algorithm performs if the measurements in each monitoring network were taken from the CFD predictions rather that the field experiment (i.e. if the error in the forward model is removed). Accordingly, the source reconstruction for each set of monitoring network was also performed from the renormalization inversion algorithm by using the data from CFD prediction (i.e. synthetic data) rather that the field experiment (i.e. real data). Synthetic data are sets of the concentration measurements predicted by a forward dispersion or an adjoint model for the known source parameters. The synthetic measurements $\boldsymbol{\mu}$ from the adjoint functions $\mathbf{a}(\mathbf{x}_0)$ are ideally generated by $\boldsymbol{\mu} = Q_0\mathbf{a}(\mathbf{x}_0)$ for the known location $\mathbf{x}_0$ and intensity Q_0 of a point source. Irrespective of the atmospheric and source conditions, synthetic measurements are free from any model and instrumental errors and are ideal for testing the inversion techniques. In the case of the synthetic measurements, the point source is estimated exactly at the same grid cell as the true source in each trial of the MUST experiment. Using the synthetic measurements from the sensors in each monitoring network, the exact estimation of the source parameters was retrieved irrespective of the varying atmospheric and source conditions in each trial of the MUST experiment. When synthetic data are used, model error vanishes and the technique was able to perfectly reconstruct the synthetic data for that idealized case.

It should be noted here that the CFD are imprecise and this implies errors associated with the predictions that are non-uniform in the space investigated. As discussed by Chow *et al.* (2008), the inversion procedure clearly relies heavily on the accuracy of the sensor measurements as well as the accuracy of the forward model used for dispersion simulations and computations of the adjoint functions. It is obvious that the errors and uncertainties associated with the CFD model prediction are concerned with the accuracy of the adjoint functions that were prerequisite and used for establishment of the optimal monitoring networks and source reconstructions in an urban-like environment. Uncertainties in the inversion procedure increase with the complexity of the domain, paralleling the errors in the adjoint model. Thus, these errors may influence the sensor placement in a monitoring network, source retrieval, etc. While the CFD code fluidyn-PANACHE has been evaluated and tested for many urban flows, there are several possible sources of error. In order to achieve a good estimation of the source location and release rate, all sources of the error must in theory be included *a priori*. As pointed out by Chow *et al.* (2008) for the source inversion in a complex urban region, model errors are sometimes difficult to control or isolate, and thus individual errors are treated as described below. There are several reasons for the mismatch in predicted and observed concentrations. Most of the observed concentrations in the MUST field experiment are averaged values from 15 to 20 min releases, whereas the CFD model predicts the steady state conditions, effectively ensemble-averaged dispersion. Thus, the shape of the plume can be different from any single realization or plume prediction, reflecting the uncertainty in the inversion procedure (Chow *et al.*, 2008). Describing the inflow boundary profiles as the steady flow introduces uncertainties in the inflow boundary conditions because in reality the wind at the domain has fluctuations in space and time. Consideration of the invariant wind direction throughout the simulation can also greatly affect the dispersion and consequently the adjoint functions for the source inversion procedure. Specification of a point source in the discretized computational domain is also a potential source of error. Errors associated with different parametrizations for the boundary conditions and turbulence model, grid resolution, etc. are also other sources of uncertainty and errors.

Despite of the errors and uncertainties associated with the CFD approach, the choice of the CFD technique in an

urban-like environment is obvious where simple analytical or Gaussian dispersion models have limitations and cannot apply to such complex environments. For homogeneous terrains, the adjoint functions can analytically be computed based on the Gaussian plume model or a simple solution of the diffusion transport equation to estimate a continuous point release. The flow-field in these models is generally considered constant throughout the computational domain. However, the flow-field in urban or industrial environments is quite complex and the asymmetry of the flow and the dispersed plume in urban regions is generated mainly by the presence of buildings and other structures. In general, the Gaussian models are unable to capture the effects of complex urban geometries on adjoint sensitivities between source and receptors. Building-resolving CFD techniques have the potential to provide the precise and realistic simulations of the wind flow and dispersion around and within the buildings and other complex structures in urban regions. A better CFD approach might lead to improvements that dominate those associated with the optimization and inversion methods. However, the complexity of the problem increases significantly by utilization of more advanced CFD techniques.

8 | CONCLUSIONS

In this study, a methodology of optimal design for fast sensor and/or mobile network deployment in emergency situations in an urban environment was presented. A cost function that quantifies the quality of a network in terms of the information for source reconstruction was defined for a particular meteorological condition. This function presents characteristics of a network using only the available meteorological measurements and it was defined without *a priori* information about the source. The space of the candidate positions for sensor deployment was defined as a discrete set and the optimization was performed to determine the best subset. This problem named combinatorial optimization was solved using the simulated annealing (SA) stochastic algorithm. The calculations were performed by coupling the CFD adjoint fields, the *renormalization* algorithm and the SA algorithm. The adjoint fields were computed using the CFD model fluidyn-PANACHE for the realistic wind flow around obstacles and to best describe the sensitivity of sensors in an urban environment. The renormalization algorithm allowed us to calculate the optimal weight function for the inverse process and to calculate the entropic criterion for the corresponding networks. The coupling is achieved successfully and optimal networks of 10 and 13 sensors based on a standard network of 40 sensors were obtained and validated for 20 trials of the MUST tracer field experiment. The results showed that the optimal networks obtained by maximizing the entropic criterion have a widely dispersed structure which leads to cover a large monitored area by the visibility fields. The quantitative results showed that the reconstruction of the source parameters for the 20 trials of the MUST experiment using optimal networks of 10 and 13 sensors is acceptable and almost comparable to the original network of 40 sensors. This confirms that the optimal design by the reduction of network size in an urban environment is possible using the entropic criterion derived from information theory and therenormalization inverse method. The comparison of the obtained optimal networks using *a priori* information as the concentration measurements with the optimal networks derived without *a priori* information of the source has highlighted the efficiency of the entropic criterion. This criterion leads to the optimal sensor networks able to reconstruct an unknown source regardless of its position or intensity according to a particular meteorological situation.

It is interesting to note that, in this study, the optimization is conducted for stationary meteorological situations during continuous releases. However, the optimal network design would also depend on the change of wind direction/speed which may increase or decrease the optimum number of sites and may also change the best positions to be instrumented by sensors. Also, the MUST array is very open (plan area coverage of less than 10%) and may not quite represent a real urban region in terms of scale, meteorological variability, non-uniform terrain or roughness/canopy structure. However, the methodology presented here is general in nature to apply also to a real urban environment. The methodology involves the utilization of the CFD model which generally can include the effects of the urban geometry, meteorological variability, non-uniform terrain or roughness/canopy structure in a real urban environment. Indeed, this work can be extended further to study the effect of the variability of the meteorological conditions in more representative urban domains.

ACKNOWLEDGEMENTS

The Mock Urban Setting Test (MUST) database is available at http://mech.utah.edu/~pardyjak/exdata/MUST.php. The authors would like to thank the Defense Threat Reduction Agency (DTRA) for providing access to the MUST field experiment dataset. The authors gratefully acknowledge Fluidyn France for use of the CFD model fluidyn-PANACHE. The authors wish to thank Dr Jean-Pierre Issartel for many useful discussions. They would like also to thank the editor and the three anonymous reviewers for their valuable comments and suggestions which improved the quality of the paper.

SUPPORTING INFORMATION

Figure S1.1. The optimal networks of 10 sensors for all 20 trials in the MUST field experiment. The blank and filled black circles respectively represent the all (40) potential positions and the optimal positions of sensors.

Figure S1.2. The optimal networks of 13 sensors for all 20 trials in the MUST field experiment. The blank and filled black circles respectively represent the all (40) potential positions and the optimal positions of sensors.

Figure S2.1. Isopleths of the renormalized weight function ($w(x)$) (grey in first and third columns) and the normalized source estimate function ($s^n_w(x = s_w(x) = \max\{s_w(x)\}$); coloured in second and fourth columns) for both optimal network respectively of 10 and 13 sensors for trials 1, 2, 3, 4, 5. The black and white filled circles respectively represent the true and estimated source locations.

Figure S2.2. Isopleths of the renormalized weight function ($w(x)$) (grey in first and third columns) and the normalized source estimate function ($s^n_w(x = s_w(x) = \max\{s_w(x)\}$); coloured in second and fourth columns) for both optimal network respectively of 10 and 13 sensors for trials 6, 7, 8, 9, 10. The black and white filled circles respectively represent the true and estimated source locations.

Figure S2.3. Isopleths of the renormalized weight function ($w(x)$) (grey in first and third columns) and the normalized source estimate function ($s^n_w(x = s_w(x) = \max\{s_w(x)\}$); coloured in second and fourth columns) for both optimal network respectively of 10 and 13 sensors for trials 11, 12, 13, 14, 15. The black and white filled circles respectively represent the true and estimated source locations.

Figure S2.4. Isopleths of the renormalized weight function ($w(x)$) (grey in first and third columns) and the normalized source estimate function ($s^n_w(x = s_w(x) = \max\{s_w(x)\}$); coloured in second and fourth columns) for both optimal network respectively of 10 and 13 sensors for trials 16, 17, 18, 19, 20. The black and white filled circles respectively represent the true and estimated source locations.

ORCID

Hamza Kouichi https://orcid.org/0000-0001-8623-2504

REFERENCES

Abida, R. and Bocquet, M. (2009) Targeting of observations for accidental atmospheric release monitoring. *Atmospheric Environment*, 43(40), 6312–6327. https://doi.org/10.1016/j.atmosenv.2009.09.029.

Abida, R., Bocquet, M., Vercauteren, N. and Isnard, O. (2008) Design of a monitoring network over France in case of a radiological accidental release. *Atmospheric Environment*, 42(21), 5205–5219. https://doi.org/10.1016/j.atmosenv.2008.02.065.

Altinel, I.K., Aras, N., Gney E and Ersoy C (2008) Binary integer programming formulation and heuristics for differentiated coverage in heterogeneous sensor networks. *Computer Networks*, 52(12), 2419–2431. https://doi.org/10.1016/j.comnet.2008.05.002.

Beljaars, A. and Holtslag, A. (1991) Flux parameterization over land surfaces for atmospheric models. *Journal of Applied Meteorology*, 30(3), 327–341. https://doi.org/10.1175/1520-0450(1991)030<0327:FPOLSF>2.0.CO;2.

Biltoft, C.A. (2001) *Customer report for Mock Urban Setting Test*. Technical report WDTC-FR-01-121. West Desert Test Center, US Army Proving Ground, Dugway, UT.

Caselton, W., Kan, L. and Zidek, J. (1992) Quality data networks that minimize entropy. In: Walden, A.T., Guttorp, P. and Arlond, E. (Eds.) *Statistics in the Environmental and Earth Sciences*. London: Edward Arnold, pp. 10–38.

Chow, F.K., Kosovic, B. and Chan, S. (2008) Source inversion for contaminant plume dispersion in urban environments using building-resolving simulations. *Journal of Applied Meteorology and Climatology*, 47(6), 1553–1572. https://doi.org/10.1175/2007JAMC1733.1.

Cohn, H. and Fielding, M. (1999) Simulated annealing: searching for an optimal temperature schedule. *SIAM Journal on Optimization*, 9(3), 779–802. https://doi.org/10.1137/S1052623497329683.

Davoine, X. and Bocquet, M. (2007) Inverse modelling-based reconstruction of the Chernobyl source term available for long-range transport. *Atmospheric Chemistry and Physics*, 7(6), 1549–1564. https://doi.org/10.5194/acp-7-1549-2007.

Dhillon, S.S. and Chakrabarty, K. (2003) Sensor placement for effective coverage and surveillance in distributed sensor networks. In: *Wireless Communications and Networking Conference 2003*, Vol. 3, pp. 1609–1614. IEEE, New Orleans, LA.

Du, K.L. and Swamy, M.N.S. (2016) Simulated Annealing. In: *Search and Optimization by Metaheuristics*. Cham: Birkhäuser. https://doi.org/10.1007/978-3-319-41192-7_2.

Efthimiou, G.C., Kovalets, I.V., Venetsanos, A., Andronopoulos, S., Argyropoulos, C.D. and Kakosimos, K. (2017) An optimized inverse modelling method for determining the location and strength of a point source releasing airborne material in urban environment. *Atmospheric Environment*, 170, 118–129. https://doi.org/10.1016/j.atmosenv.2017.09.034.

Fluidyn-Panache (2010) *User Manual*, FLUIDYN France/TRANSOFT International, version 4.0.7. https://www.fluidyn.com/fluidyn/panache

Gryning, S.E., Batchvarova, E., Brummer, B., Jorgensen, H. and Larsen, S. (2007) On the extension of the wind profile over homogeneous terrain beyond the surface boundary layer. *Boundary-Layer Meteorology*, 124(2), 251–268. https://doi.org/10.1007/s10546-007-9166-9.

Hajek, B. (1987) *Cooling Schedules for Optimal Annealing*. New York, NY: Springer.

Hanjalic, K. (2005) Turbulence and transport phenomena: modelling and simulation. In: *Turbulence Modeling and Simulation (TMS) Workshop*. Technische Universit'at Darmstadt, Germany. http://www.academia.edu/22152743/TURBULENCE_AND_TRANSPORT_PHENOMENA_Modelling_and_Simulation

Hourdin, F. and Issartel, J.P. (2000) Sub-surface nuclear tests monitoring through the CTBT xenon network. *Geophysical Research Letters*, 27(15), 2245–2248. https://doi.org/10.1029/1999GL010909.

Hourdin, F. and Talagrand, O. (2006) Eulerian backtracking of atmospheric tracers. I: Adjoint derivation and parametrization of subgrid-scale transport. *Quarterly Journal of the Royal Meteorological Society*, 132, 567–583. https://doi.org/10.1256/qj.03.198.A.

Hutchinson, M., Oh, H. and Chen, W.H. (2017) A review of source term estimation methods for atmospheric dispersion events using static or mobile sensors. *Information Fusion*, 36(Supplement C), 130–148. https://doi.org/10.1016/j.inffus.2016.11.010.

Issartel, J.P. (2005) Emergence of a tracer source from air concentration measurements, a new strategy for linear assimilation. *Atmospheric Chemistry and Physics*, 5(1), 249–273. https://doi.org/10.5194/acp-5-249-2005.

Issartel, J.P. and Baverel, J. (2003) Inverse transport for the verification of the comprehensive nuclear test ban treaty. *Atmospheric Chemistry and Physics*, 3(3), 475–486. https://doi.org/10.5194/acp-3-475-2003.

Jiang, Z., de Bruin, S., Heuvelink, G. and Twenhöfel, C. (2007) Optimization of mobile radioactivity monitoring networks. In: *Fifth International Symposium on Spatial Data Quality*, Enschede, The Netherlands

Kaminski, T. and Heimann, M. (2001) Inverse modeling of atmospheric carbon dioxide fluxes. *Science*, 294(5541), 259–259. https://doi.org/10.1126/science.294.5541.259a.

Keats, W.A. (2009) *Bayesian inference for source determination in the atmospheric environment*. PhD thesis, University of Waterloo, Ontario, Canada. Available at: http://hdl.handle.net/10012/4317 [Accessed 30th January 2019]

Kirkpatrick, S., Gelatt, C.D. and Vecchi, M.P. (1983) Optimization by simulated annealing. *Science*, 220(4598), 671–680. https://doi.org/10.1126/science.220.4598.671.

Ko, C.W., Lee, J. and Queyranne, M. (1995) An exact algorithm for maximum entropy sampling. *Operations Research*, 43(4), 684–691. https://doi.org/10.1287/opre.43.4.684.

Kouichi, H. (2017) *Sensor network optimization for the characterization of the source of atmospheric releases*. Thesis, Université Paris Saclay, France. Available at: https://hal.archives-ouvertes.fr/tel-01593834 [Accessed 30th January 2019]

Kouichi, H., Turbelin, G., Ngae, P., Feiz, A., Barbosa, E. and Chpoun, A. (2016) Optimization of sensor networks for the estimation of atmospheric pollutant sources. *WIT Transactions on Ecology and the Environment*, 207, 11–21.

Kouichi, H., Ngae, P., Kumar, P., Feiz, A.A. and Bekka, N. (2018) Optimization of an urban monitoring network for retrieving an unknown point source emission.

Geoscientific Model Development Discussions, 1–24. https://doi.org/10.5194/gmd-2018-6.

Kovalets, I.V., Andronopoulos, S., Venetsanos, A.G. and Bartzis, J.G. (2011) Identification of strength and location of stationary point source of atmospheric pollutant in urban conditions using computational fluid dynamics model. *Mathematics and Computers in Simulation*, 82(2), 244–257. https://doi.org/10.1016/j.matcom.2011.07.002.

Kumar, P., Feiz, A.A., Ngae, P., Singh, S.K. and Issartel, J.P. (2015a) CFD simulation of short-range plume dispersion from a point release in an urban-like environment. *Atmospheric Environment*, 122, 645–656. https://doi.org/10.1016/j.atmosenv.2015.10.027.

Kumar, P., Feiz, A.A., Singh, S.K., Ngae, P. and Turbelin, G. (2015b) Reconstruction of an atmospheric tracer source in an urban-like environment. *Journal of Geophysical Research: Atmospheres*, 120(24), 12589–12604. https://doi.org/10.1002/2015JD024110.

Kumar, P., Singh, S.K., Feiz, A.A. and Ngae, P. (2016) An urban-scale inverse modelling for retrieving unknown elevated emissions with building-resolving simulations. *Atmospheric Environment*, 140, 135–146. https://doi.org/10.1016/j.atmosenv.2016.05.050.

Launder, B. (2004) *Turbulence modelling of buoyancy-affected flows*. Presentation at Turbulence Colloquium, Singapore. Available at: https://www.slideserve.com/bill/turbulence-modelling-of-buoyancy-affected-flows [Accessed 30th January 2019]

Le, N.D. and Zidek, J.V. (1994) Network designs for monitoring multivariate random spatial fields. In: Vilaplana, J.P. and Puri, M.L. (Eds.) *Recent Advances in Statistics and Probability; Proceedings of the 4th International Meeting of Statistics in the Basque Country, San Sebastián, Spain, 4–7 August 1992*. San Sebastián, Spain: V S P Intl Science, pp. 191–206.

Lepley, J.J. and Lloyd, D.R. (2010) A rapidly deployable chemical sensing network for the real-time monitoring of toxic airborne contaminant releases in urban environments. In: *Proceedings of Chemical, Biological, Radiological, Nuclear, and Explosives (CBRNE) Sensing XI*, Orlando, FL, Society of Photo-Optical Instrumentation Engineers, p. 76650E.

Lepley, J.J., Lloyd, D.R., Robins, A., Rudd, A. and Wilks, A. (2011) Dynamic sensor deployment for the monitoring of chemical releases in urban environments (DYCE). In: *Proceedings of Chemical, Biological, Radiological, Nuclear, and Explosives (CBRNE) Sensing XII*, Orlando, FL, Society of Photo-Optical Instrumentation Engineers, p. 801812

Luhar, A.K., Etheridge, D.M., Leuning, R., Loh, Z.M., Jenkins, C.R. and Yee, E. (2014) Locating and quantifying greenhouse gas emissions at a geological CO2 storage site using atmospheric modeling and measurements. *Journal of Geophysical Research: Atmospheres*, 119(18), 10959–10979. https://doi.org/10.1002/2014JD021880.

Ma, D., Deng, J. and Zhang, Z. (2013) Comparison and improvements of optimization methods for gas emission source identification. *Atmospheric Environment*, 81(Supplement C), 188–198. https://doi.org/10.1016/j.atmosenv.2013.09.012.

Marchuk, G.I. (1995) *Adjoint Equations and Analysis of Complex Systems*. Dordrecht: Springer.

Mason, L.R. and Bohlin, J.B. (1995) *Optimization of an atmospheric radionuclide monitoring network for verification of the Comprehensive Nuclear Test Ban Treaty*. Technical Report 2585, Pacific-Sierra Research Corporation, Arlington, VA.

Metropolis, N., Rosenbluth, A.W., Rosenbluth, M.N., Teller, A.H. and Teller, E. (1953) Equation of state calculations by fast computing machines. *Journal of Chemical Physics*, 21(6), 1087–1092.

Mini, S., Udgata, S.K. and Sabat, S.L. (2011) Artificial bee colony-based sensor deployment algorithm for target coverage problem in 3D terrain. In: Natarajan, R. and Ojo, A. (Eds.) *Proceedings of International Conference on Distributed Computing and Internet Technology*. pp. 313–324, *Bhubaneshwar, India*. Berlin: Springer.

Monache, L.D., Lundquist, J.K., Kosovi B, Johannesson G, Dyer KM, Aines RD, Chow FK, Belles RD, Hanley WG, Larsen SC, Loosmore GA, Nitao JJ, Sugiyama GA and Vogt PJ (2008) Bayesian inference and Markov chain Monte-Carlo sampling to reconstruct a contaminant source on a continental scale. *Journal of Applied Meteorology and Climatology*, 47(10), 2600–2613. https://doi.org/10.1175/2008JAMC1766.1.

National Research Council (2010) *Acute Exposure Guideline Levels for Selected Airborne Chemicals*, Vol. 9. Washington, DC: NRC Committee on Acute Exposure Guideline Levels, National Academies Press.

Nourani, Y. and Andresen, B. (1998) A comparison of simulated annealing cooling strategies. *Journal of Physics A: Mathematical and General*, 31(41), 8373–8385. https://doi.org/10.1088/0305-4470/31/41/011.

Nychka, D. and Saltzman, N. (1998) *Design of Air-Quality Monitoring Networks*. New York, NY: Springer.

Pudykiewicz, J.A. (1998) Application of adjoint tracer transport equations for evaluating source parameters. *Atmospheric Environment*, 32(17), 3039–3050. https://doi.org/10.1016/S1352-2310(97)00480-9.

Rao, K.S. (2007) Source estimation methods for atmospheric dispersion. *Atmospheric Environment*, 41(33), 6964–6973. https://doi.org/10.1016/j.atmosenv.2007.04.064.

Saunier, O., Bocquet, M., Mathieu, A. and Isnard, O. (2009) Model reduction via principal component truncation for the optimal design of atmospheric monitoring networks. *Atmospheric Environment*, 43(32), 4940–4950. https://doi.org/10.1016/j.atmosenv.2009.07.011.

Seibert, P. (2001) Inverse modelling with a Lagrangian particle disperion model: application to point releases over limited time intervals. In: Gryning, S.-E. and Schiermeier, F.A. (Eds.) *Air Pollution Modeling and Its Application XIV*. pp. 381–389. New York, NY: Kluwer/Plenum.

Shannon, C.E. and Weaver, W. (1998) *The Mathematical Theory of Communication*. Champaign, IL: University of Illinois Press.

Sharan, M. and Kumar, P. (2010) Estimation of upper bounds for the applicability of non-linear similarity functions for non-dimensional wind and temperature profiles in the surface layer in very stable conditions. *Proceedings of the Royal Society of London A: Mathematical, Physical and Engineering Sciences*, 467(2126), 473–494. https://doi.org/10.1098/rspa.2010.0220.

Sharan, M., Issartel, J.P., Singh, S.K. and Kumar, P. (2009) An inversion technique for the retrieval of single-point emissions from atmospheric concentration measurements. *Proceedings of the Royal Society of London A: Mathematical, Physical and Engineering Sciences*, 465, 2069–2088. https://doi.org/10.1098/rspa.2008.0402.

Siarry, P. (2014) *Métaheuristiques: Recuits simulé, recherche avec tabous, recherche à voisinages variables, méthodes grasp, algorithmes évolutionnaires, fourmis artificielles, essaims particulaires et autres méthodes d'optimisation*. Paris: Editions Eyrolles.

Wu, Y., Li, M., Cai, Z. and Zhu, E. (2008) A distributed algorithm to approximate node-weighted minimum α-connected (θ, k)-coverage in dense sensor networks. In: Preparata, F.P., Wu, X. and Yin, J. (Eds.) *Second International Workshop on Frontiers in Algorithmics, Changsha, China*. Berlin: Springer, pp. 221–232.

Yang, Y., Gu, M., Chen, S. and Jin, X. (2009) New inflow boundary conditions for modelling the neutral equilibrium atmospheric boundary layer in computational wind engineering. *Journal of Wind Engineering and Industrial Aerodynamics*, 97(2), 88–95. https://doi.org/10.1016/j.jweia.2008.12.001.

Yee, E. and Biltoft, C. (2004) Concentration fluctuation measurements in a plume dispersing through a regular array of obstacles. *Boundary-Layer Meteorology*, 111(3), 363–415. https://doi.org/10.1023/B:BOUN.0000016496.83909.ee.

Yee, E., Hoffman, I. and Ungar, K. (2014) Bayesian inference for source reconstruction: a real-world application. *International Scholarly Research Notices*, 2014, 1–12. https://doi.org/10.1155/2014/507634.

Zhang, X.L., Su, G.F., Chen, J.G., Raskob, W., Yuan, H.Y. and Huang, Q.Y. (2015) Iterative ensemble Kalman filter for atmospheric dispersion in nuclear accidents: an application to Kincaid tracer experiment. *Journal of Hazardous Materials*, 297(Supplement C), 329–339. https://doi.org/10.1016/j.jhazmat.2015.05.035.

Zidek, J.V., Sun, W. and Le, N.D. (2000) Designing and integrating composite networks for monitoring multivariate Gaussian pollution fields. *Journal of the Royal Statistical Society: Series C (Applied Statistics)*, 49(1), 63–79. https://doi.org/10.1111/1467-9876.00179.